

Evaluation of Neutronic and Thermophysical Characteristics of Molten Salts Specialized for Long-Lived Fission Products Transmutation in a Fusion Reactor^{*)}

Taku KITASAKA, Hiroki SHISHIDO and Hidetoshi HASHIZUME

Department of Quantum Science and Energy Engineering, Graduate School of Engineering, Tohoku University, Sendai 980-8579, Japan

(Received 29 November 2019 / Accepted 15 June 2020)

This study proposes new molten salts, which are specialized for transmuting long-lived fission products (LLFP) using a helical fusion reactor FFHR-d1, as a neutron source. Molten salts are binary systems consisting of BeF_2 and LLFP fluorides, such as $\text{BeF}_2\text{-ZrF}_2$, $\text{BeF}_2\text{-PdF}_4$, or $\text{BeF}_2\text{-CsF}$. This study evaluates the effect of molten salts on the transmutation performance, and the amount of heat generated was evaluated by Monte Carlo-based neutron transport and burnup calculations. Therefore, when the transmutation area was fixed at 4% of the blanket system volume, the higher molar ratio of LLFP fluorides leads to higher transmutation performance. Also, the viscosity, specific heat, and thermal conductivity of $\text{BeF}_2\text{-CsF}$ were evaluated by molecular dynamics (MD) simulations. The heat transfer characteristics were evaluated by calculating the Prandtl number from MD simulation results. The Prandtl number of 50% CsF, which produced the lowest melting point (475°C), was evaluated to be 29.23, which was 60% larger compared to the Prandtl number of Flibe (LiF-BeF_2) when the BeF_2 molar ratio was 50%. This result suggested that the heat transfer performance was inferior to that of Flibe.

© 2020 The Japan Society of Plasma Science and Nuclear Fusion Research

Keywords: Monte Carlo method, burnup calculation, molecular dynamics, BeF_2 , Prandtl number, LLFP

DOI: 10.1585/pfr.15.2405077

1. Introduction

The disposal of undesirable high-level radioactive waste is a major issue with fission-based nuclear energy. LLFP is one factor that is responsible for radioactivity and decay heat of the high-level radioactive waste. Thus far, the studies evaluated geological disposal as the most practical solution, and the storage of high-level waste for a long time suffers from safety uncertainties. The nuclear transmutation of LLFP into non-radioactive or short-lived nuclides has been considered as an alternative approach to diminishing the radiological impact of waste. The neutron source candidates for transmutation include fast reactors [1], accelerator-driven systems [2], and fusion reactors [3, 4]. Among these candidates, fusion reactors have might be the most efficient system to transmute LLFP owing to their neutron environment (e.g., flexibility to design a neutron flux and spectrum [5]) and the availability of neutrons compared to other neutron sources.

There has been a proposal to mix LLFP into a Flibe (LiF-BeF_2) blanket system in fusion reactors to transmute LLFP [6]. However, to maintain the tritium breeding ratio (TBR), the amount of LLFP added to the fusion blanket is insufficient to contribute to the nuclear cycle. As a solution, this study proposes new molten salts that are

specialized for LLFP transmutation. The molten salts consist of LLFP fluorides and BeF_2 because BeF_2 has a low melting point, low neutron absorption, and high neutron multiplication cross-section. By adding larger amounts of LLFP and arranging the molten salts in very limited regions of the blanket system, it may be possible to maintain the net TBR and increase the amount of LLFP transmutation. Because LLFP fluorides cannot be mixed if LLFP fluorides are gas at the blanket temperature of 500°C, the target LLFP was ^{93}Zr , ^{107}Pd , and ^{135}Cs . There are few reports on the thermophysical properties of binary salts such as $\text{BeF}_2\text{-CsF}$. Although they are effective from the viewpoint of LLFP annihilation, the feasibility of thermal design in a self-cooled liquid blanket is not clear.

This study aimed to evaluate the feasibility of molten salts specialized for the LLFP transmutation from the viewpoint of neutronics and heat transfer characteristics. Neutron transport and burnup calculations were conducted to evaluate the transmutation performance of the new molten salt. Subsequent molecular dynamics (MD) simulations were performed to evaluate specific heat, viscosity, and thermal conductivity of the molten salt. Furthermore, the heat transfer performance was evaluated by calculating the Prandtl number based on the MD simulation results and compared to the conventional candidate Flibe.

author's e-mail: takukitasaka@gmail.com

^{*)} This article is based on the presentation at the 28th International Toki Conference on Plasma and Fusion Research (ITC28).

2. Neutron Transport and Burnup Analysis

2.1 Analysis methods and conditions

The transmutation rate of the target LLFP ^{93}Zr , ^{107}Pd , and ^{135}Cs and the amount of heat generated were evaluated using neutron transport and burnup analysis. Figure 1 shows a simple geometry model of the FFHR-d1 [7] blanket system used in the simulations. Materials and the size of each section are also shown in Fig. 1. The fusion plasma was simulated by a neutron source emitting at 14.06 MeV in the z-direction. The neutron source was set apart from $Z = 0$ to avoid overlap of the neutron source and mirror reflection. The neutron wall loading was set to 1.5 MW/m² based on the FFHR-d1 design, which has a thermal output of 3 GW. The transmutation region was divided into two zones; only the first 15 cm contained Be as the neutron multiplier material. All regions homogeneously contained the structure material JLF-1 [Fe (bal.), Cr (9.04), W (1.97), V (0.19), Ta (0.07), C (0.097), Mn (0.46), N (0.05) (wt.%) [8] at 10% volume ratio. The LLFP fluoride molar ratio was changed within the range of 10% - 90%. The isotopic composition of each LLFP shown in Table 1 was based on the data on the spent fuel from a pressurized water reactor with a burnup of 45 GWd/t and 30 years of cooling [9]. The GWd/t unit indicates the burnup of fuel, where d is day, and t is ton. It is the exact released energy by fission reaction per the initial weight of the fuel.

Figure 2 shows the transmutation area in FFHR-d1. An earlier study has proposed that the region was promising for transmutation for the following reasons: sufficient neutron flux (< 2 MW/m²) and lower heat flux than the region inside the helical coils. Because minor actinides will

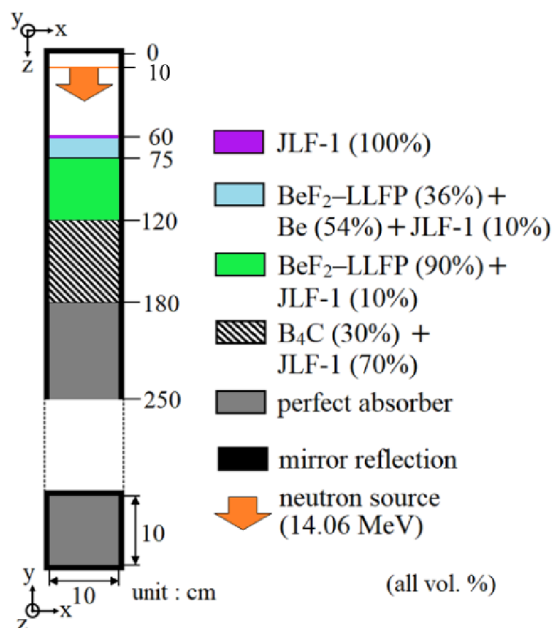


Fig. 1 Neutron transport and burnup simulation geometry model.

be placed downside of the plasma in case of a severe accident [10], LLFP will be placed upside of the plasma. Then, 10 loading positions, which are 4% of the blanket system volume, are secured in one helical-type fusion reactor, which has five helical pitches designed in FFHR-d1, as shown in Fig. 3. The TBR of FFHR-d1 is reportedly 1.08 [11] when using Flibe as the tritium breeder. Because the new molten salts cannot breed tritium, the TBR of the entire reactor will decrease; however, because the transmutation area is limited, the TBR is estimated to be above 1.0. Figure 3 shows the simulation geometry in the right bottom. The neutron source position corresponded to the last closed flux surface.

The simulations were conducted using the neutron transport calculation code MVP-2.0 [12], based on the Monte Carlo method and the MVP-BURN [13] module, to evaluate the transmutation rate and generated heat. The cross-section data library JENDL4.0 [14] was used for the simulations. The number of histories for neutron transport

Table 1 Isotopic composition.

Element	Isotope	Isotopic composition [%]
Zr	^{90}Zr	7.90
	^{91}Zr	15.45
	^{92}Zr	16.70
	^{93}Zr	18.73
	^{94}Zr	20.09
	^{96}Zr	21.13
	Total	100.00
Pd	^{104}Pd	17.67
	^{105}Pd	26.46
	^{106}Pd	26.43
	^{107}Pd	15.72
	^{108}Pd	10.57
	^{110}Pd	3.15
	Total	100.00
Cs	^{133}Cs	52.26
	^{134}Cs	2.85×10^{-4}
	^{135}Cs	18.32
	^{137}Cs	29.42
	Total	100.00

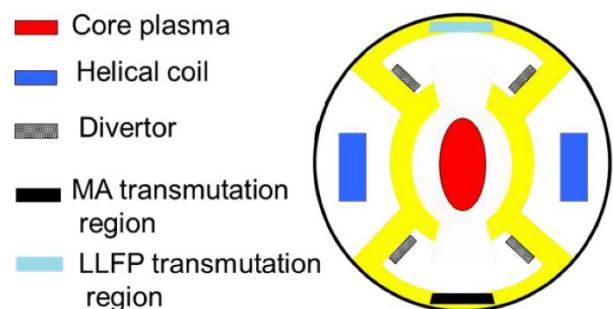


Fig. 2 Transmutation areas in the poloidal cross-section of FFHR-d1.

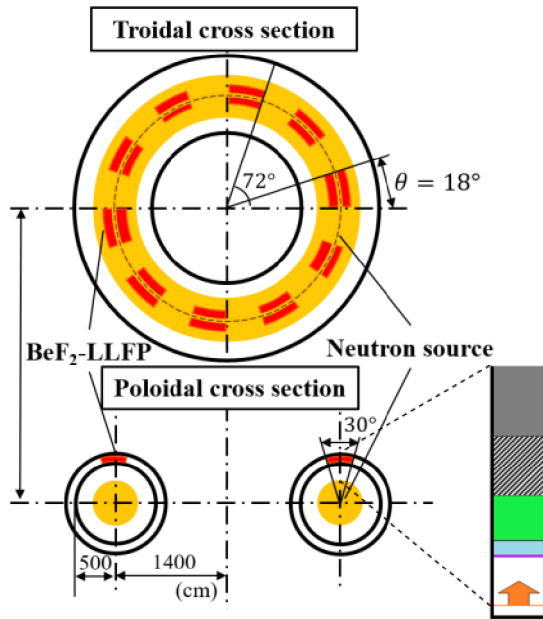


Fig. 3 Toroidal and poloidal view of the transmutation area in FFHR-d1 and the geometry model in the simulation.

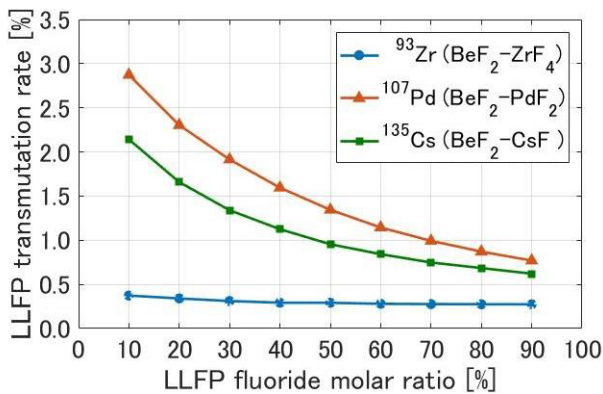


Fig. 4 Transmutation rate of each LLFP after a 1-year operation.

simulations was set to 100,000 so that the statistical errors of neutron flux were less than 1.0%.

2.2 Results

Figure 4 shows the result of the transmutation rate of ^{93}Zr , ^{107}Pd , and ^{135}Cs after 1 year of fusion neutron irradiation. The transmutation rate decreases as the LLFP fluoride molar ratio increases. The transmutation amount of each LLFP in the geometry, shown in Fig. 1, was calculated based on the transmutation rate. Figure 5 shows the results of the transmutation amount. An increase in the LLFP fluoride ratio led to an increase in the transmutation amount. Table 2 shows the annual change rate of the isotopes of each LLFP when the LLFP fluoride molar ratio is 10%. The change rate is the increase or decrease of each isotope after 1-year transmutation. All LLFP (^{93}Zr , ^{107}Pd , and ^{135}Cs) decrease and all increasing isotopes are stable or have a short half-life. The obtained results indicated that

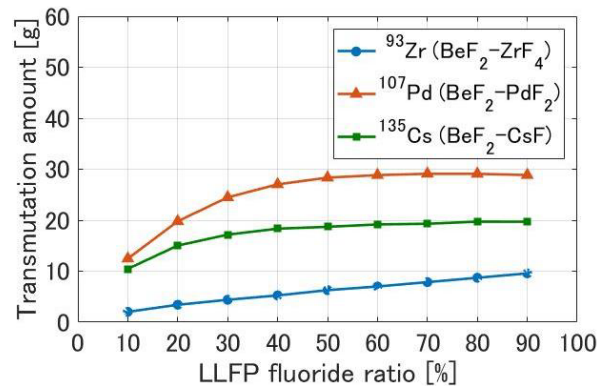


Fig. 5 Transmuted amount of each LLFP in the geometry shown in Fig. 1.

Table 2 Isotope data (LLFP fluoride ratio 10%).

Element	Isotope	Half-life [year]	Change rate [%]
Zr	^{90}Zr	Stable	+0.31
	^{91}Zr	Stable	-0.15
	^{92}Zr	Stable	+0.48
	^{93}Zr	1.53×10^6	-0.32
	^{94}Zr	Stable	+0.51
	^{96}Zr	2.00×10^{19}	-0.25
Pd	^{104}Pd	Stable	-0.55
	^{105}Pd	Stable	-1.98
	^{106}Pd	Stable	+2.34
	^{107}Pd	6.50×10^6	-2.57
	^{108}Pd	Stable	+2.97
	^{110}Pd	Stable	-0.24
Cs	^{133}Cs	Stable	-3.88
	^{134}Cs	2.07	$+3.71 \times 10^5$
	^{135}Cs	2.30×10^6	-1.97
	^{137}Cs	30.17	-3.80

transmutation was qualitatively efficient.

The support factor of each LLFP was estimated based on the obtained transmutation rate. The support factor was defined as the ratio of the transmuted amount of LLFP by a fusion reactor to the annual produced amount of LLFP from one unit of 1-GWe class light water reactor. Figure 6 shows the LLFP support factor. The loading volume ratio of each salt was also calculated based on the obtained transmutation rate. The total blanket system volume, as shown in Fig. 2, and the loading volume ratio of each molten salt was adjusted to make the support factor of ^{93}Zr , ^{107}Pd , ^{135}Cs the same. Table 3 shows the loading volume ratios for the salts. Similar to the transmutation amount shown in Fig. 5, the transmutation performance increases with an increase in the molar ratio, and it was the highest at the support factor of 6.0 when the molar ratio of LLFP fluorides was 90%.

Figure 7 shows the amount of generated heat, which is the total amount of reaction heat and decay heat when the molar fraction of LLFP fluorides was changed. The gen-

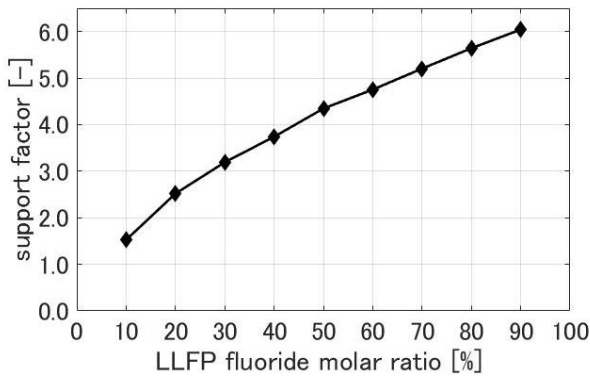


Fig. 6 Support factor (4% vol. ratio loading, 3 GWth).

Table 3 Loading area ratio for each molten salt.

LLFP ratio [mol. %]	Loading area [blanket vol. %]			
	ZrF ₄	PdF ₂	CsF	Total
10	3.44	0.17	0.39	4.00
20	3.37	0.18	0.45	4.00
30	3.32	0.18	0.50	4.00
40	3.26	0.20	0.54	4.00
50	3.16	0.22	0.62	4.00
60	3.10	0.24	0.66	4.00
70	3.03	0.25	0.72	4.00
80	2.96	0.28	0.76	4.00
90	2.88	0.30	0.82	4.00

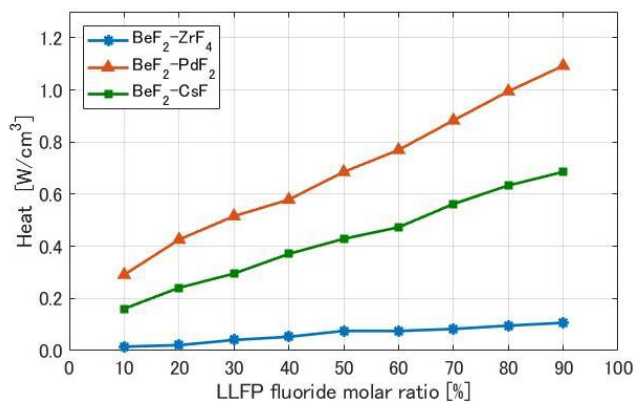


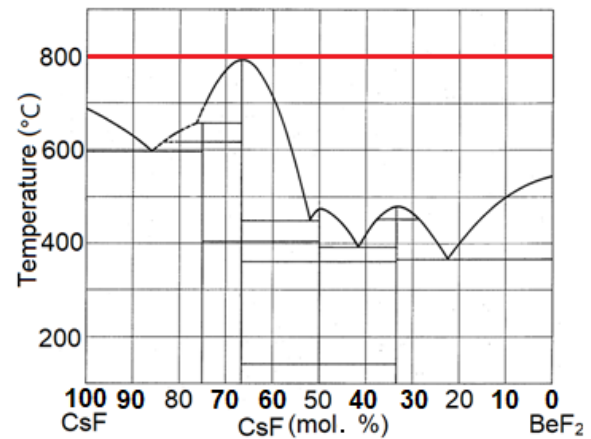
Fig. 7 Generated heat through transmutation.

erated heat amount gradually increases with an increase in the LLFP fluoride ratio. The salt BeF₂-PdF₂ has the largest amount of 1.09 W/cm³ because Pd nuclides captured more neutrons than Zr and Cs nuclides. This amount is not too large compared to the estimated heat density of the molten salt reactor core of 70 W/cm³ [15].

3. Molecular Dynamics Simulations

3.1 Simulation methods and conditions

MD simulations with the polarizable ion model potentials [16] were performed to evaluate the viscosity, specific heat, and thermal conductivity of BeF₂-CsF. BeF₂-CsF was chosen because ¹³⁵Cs is one of the most prob-


 Fig. 8 Phase diagram of BeF₂-CsF [21].

lematic LLFP because of the high risk that it may dissolve into the groundwater during geological disposal. The temperature was set to 800°C to make sure that the molten salt was liquid under all conditions to determine the trends of Prandtl number, depending on the CsF molar ratio, as shown in Fig. 8. The CsF molar fraction changed to 50%, 60%, 70%, 80%, and 100%. Molar fractions below 50% were not evaluated because the calculation would require a very long time to converge. Also, the Prandtl number of 50% CsF was evaluated and compared to FLiBe. This condition was selected because under the condition of BeF₂ molar ratio lower than 50%, 50% CsF produces a relatively low melting point (475°C) among the points calculated in this study. The temperature was set to 600°C to compare with literal values. The potential parameters in the polarizable ion model were determined from first-principles calculations in earlier studies [17, 18].

MD simulations for the specific heat were conducted in the ensemble of fixed ion number, pressure, and temperature following the method described by earlier studies [18, 19]. The simulation cells were fixed at 0 GPa. The time step was 0.5 fs, and the total simulation time was 500 ps. Simulations were performed at 600, 700, and 800°C to calculate the specific heat and evaluate system enthalpy. A linear relationship between enthalpy and temperature was obtained for all cases. The specific heat was calculated by temperature differential of the enthalpy.

The viscosity and thermal conductivity were calculated by Green-Kubo relations [20]. The simulations for viscosity and thermal conductivity were performed in the ensemble of fixed ion number, cell size, and temperature. The cell volume was determined from the results of the simulation to obtain density. A series of 250-ps production runs were performed until the transport coefficients converged. Table 4 summarizes the compositions and number of ions of the molten salt for MD simulations.

The Prandtl number, Pr, was calculated from the MD simulation results as

$$\text{Pr} = \frac{\eta C_p}{\lambda}, \quad (1)$$

Table 4 Composition and number of ions in the molten salt.

Composition of		Number of ions		
BeF ₂ : CsF	Be ²⁺	Cs ⁺	F ⁻	
50: 50	100	100	300	
40: 60	84	126	294	
30: 70	66	154	286	
20: 80	46	184	276	
0: 100	0	256	256	

where η is the viscosity, C_p is the specific heat, and λ is the thermal conductivity. This study used the Prandtl number as an indicator for the heat transfer performance and compared the results with the conventional salt Flibe.

3.2 Results

Table 5 shows the calculated physical properties, Prandtl number of the molten salts, and experimental data of CsF reported in [22–24]. The calculated properties of CsF differed from the experimental values; the difference between them was 42% at most. Table 5 shows that viscosity depends on the BeF₂ ratio, which is the same trend as that for Flibe [25]. BeF₂ forms glassy tetrahedra, which results in high viscosity. The Prandtl number considerably depended on the BeF₂ ratio owing to an increase in viscosity and specific heat. The standard errors in the calculations were below 2.9% for viscosity and below 2.8% for specific heat. However, the standard error of thermal conductivity (which is summarized in Table 6) was large and increased with an increase in the molar ratio of BeF₂. This occurred because of the error propagation of the transport coefficients. The thermal conductivity λ was calculated using:

$$\lambda = \frac{1}{T^2} \left(L_{ee} - \frac{L_{ez_0} A_{z_0 z_1} + L_{ez_1} A_{z_1 z_0}}{B} \right), \quad (2)$$

$$A_{\alpha\beta} = \begin{vmatrix} L_{e\alpha} & L_{\beta\alpha} \\ L_{e\beta} & L_{\beta\beta} \end{vmatrix}, B = \begin{vmatrix} L_{z_0 z_0} & L_{z_1 z_0} \\ L_{z_0 z_1} & L_{z_1 z_1} \end{vmatrix}, \quad (3)$$

where T is the temperature, and L is the transport coefficients [26]. Several transport coefficients are necessary to calculate the thermal conductivity, as shown in Eqs. (2) and (3). The transport coefficients excessively fluctuated and contained calculation errors; this resulted in a considerable standard error for thermal conductivity evaluation. The standard error was large. There was a tendency for the thermal conductivity to increase with an increase in the molar ratio of CsF.

Table 7 shows the Prandtl number at 600°C, which was evaluated by MD simulations and the melting point of BeF₂–CsF (CsF 50%), Flibe (BeF₂ 50%), and Flibe (BeF₂ 33%). As shown in Table 7, the Prandtl number of BeF₂–CsF was 27.57, which was 50% higher than that of Flibe (BeF₂ 50%) and three times higher than that of Flibe (BeF₂ 33%). This means that the BeF₂–CsF molten salt heat transfer performance is inferior compared to that of Flibe. This comparison shows that it will be difficult to use the

Table 5 Results of MD simulations (800°C).

CsF [mol. %]	Viscosity [mPa·s]	Specific heat [J/kg·K]	Thermal conductivity [W/m·K]	Prandtl Number [-]
50	4.31	905.52	0.25	15.45
60	2.91	740.66	0.21	10.18
70	1.93	632.15	0.21	5.86
80	1.29	532.49	0.22	3.12
100	0.91	448.53	0.27	1.50
100 (exp. data)	1.22 [22]	487.52 [23]	0.48 [24]	

Table 6 Results of thermal conductivity and standard error (800°C).

CsF ratio [mol. %]	Thermal conductivity [W/m·K]	Standard error [W/m·K]
50		97.46
60		106.96
70		38.88
80		6.61
100		0.05
100 (exp. data)	0.48 [24]	

Table 7 Prandtl number at 600°C evaluated by MD simulations and melting point of the molten salts.

Molten salt	Melting point [°C]	Prandtl number [-]
BeF ₂ –CsF (CsF 50%)	475	29.23
Flibe (BeF ₂ 50%) [25]	364	17.97
Flibe (BeF ₂ 33%) [25]	459	9.13

BeF₂–CsF molten salt as a coolant for the first wall, and it is necessary to consider the effect on the thermal design of the blanket.

4. Conclusion

This study evaluated the feasibility of using molten salts specialized for the transmutation of ⁹³Zr, ¹⁰⁷Pd, and ¹³⁵Cs from the viewpoint of neutronics and heat transfer characteristics. Neutron transport and burnup calculations results confirmed that higher transmutation performance could be expected when the LLFP molar ratio is higher. The highest support factor was 6.0 when the molar ratio of LLFP fluorides was 90%. The molten salt BeF₂–PdF₂ generated the largest amount of heat of 1.09 W/cm³. This amount is not too large for the molten salt blanket system. The MD simulation results confirm that the Prandtl number of BeF₂–CsF tends to increase with an increase in the molar ratio of BeF₂. The Prandtl number of 50% CsF was 29.23; the value was 60% larger than Flibe when the BeF₂ molar ratio was 50%. The result indicated that it could be difficult to design a blanket system using the BeF₂–CsF

molten salt as a first wall coolant. Thereby the effect on the thermal design of the blanket system needs to be evaluated.

Acknowledgments

The authors would like to thank N. Ohtori for advice on molecular dynamics simulations. This study was partly supported by JSPS KAKENHI Grant Number JP17H06231

- [1] S. Chiba *et al.*, *Sci. Rep.* **7**, 13961 (2017).
- [2] Z. Chen *et al.*, *Ann. Nucl. Energy* **75**, 723 (2015).
- [3] T. Parish *et al.*, *Nucl. Technol.* **47**, 324 (1980).
- [4] E.T. Cheng, *Fusion Technol.* **39**, 530 (2001).
- [5] A. Takibayev *et al.*, *Prog. Nucl. Energy* **47**, 354 (2005).
- [6] Y. Gohar, *Fusion Technol.* **39**, 535 (2001).
- [7] A. Sagara *et al.*, *Fusion Eng. Des.* **87**, 594 (2012).
- [8] H. Tanigawa *et al.*, *J. Plasma Fusion Res.* **87**, 167 (2011).
- [9] Y. Ando *et al.*, *JAERI-Research* 99-004 (1999).
- [10] Y. Furudate *et al.*, *Prog. Nucl. Energy* **193**, 28 (2018).
- [11] T. Tanaka *et al.*, Neutronic design of helical type DEMO reactor FFHR-d1, 24th IAEA Fusion Energy Conference (2012).
- [12] Y. Nagaya *et al.*, *JAERI* 1348 (2005).
- [13] K. Okumura *et al.*, *J. Nucl. Sci. Technol.* **37**, 128 (2000).
- [14] K. Shibata *et al.*, *J. Nucl. Sci. Technol.* **48**, 1 (2011).
- [15] AESJ, Molten salt breeder reactors, Report of technical committee on molten salt breeder reactor research (1981).
- [16] M. Salanne *et al.*, *Mol. Phys.* **109**, 2299 (2011).
- [17] Y. Ishii *et al.*, *Mol. Phys.* **113**, 2442 (2015).
- [18] H. Shishido *et al.*, *Fusion Sci. Technol.* **68**, 669 (2015).
- [19] G. Martina *et al.*, *J. Chem. Phys.* **101**, 4177 (1994).
- [20] J.P. Hansen and I.R. McDonald, *Theory of Simple Liquids, 3rd Edition* (Academic Press, London, 2006).
- [21] R. Thoma, ORNL-2548 (1959).
- [22] T. Ejima *et al.*, *J. Jpn. Inst. Met.* **51**, 328 (1987).
- [23] M.W. Chase, Jr., *J. Phys. Chem. Ref. Data, Monograph* **9**, 1963 (1998).
- [24] M. Smirnov *et al.*, *Electrochimica Acta* **32**, 1019 (1987).
- [25] H. Shishido, Tohoku University Doctoral thesis (2017).
- [26] Y. Ishii *et al.*, *J. Phys. Chem. B* **118**, 3385 (2014).